

Superconductivity of β -Gallium

Yundi Quan,^{1,2,3} P. J. Hirschfeld,¹ and R. G. Hennig^{2,3}

¹*Department of Physics, University of Florida, Gainesville, Florida 32611, USA*

²*Department of Materials Science and Engineering,
University of Florida, Gainesville, Florida 32611, USA*

³*Quantum Theory Project, University of Florida, Gainesville, Florida 32611, USA*

(Dated: April 21, 2021)

Elemental gallium can exist in several phases under ambient conditions. The stable α phase has a superconducting transition temperature, T_c , of 0.9 K. By contrast, the T_c of the metastable β phase is around 6 K. To understand the significant improvement in T_c in the β phase, we first calculate the electronic structure, phonon dispersion, and the electron-phonon coupling of gallium in the α and β phase. Next, we solve the Eliashberg equations to obtain the superconducting gaps and the transition temperatures. Using these results, we relate the increased T_c in the β phase to structural differences between the phases that affect the electronic and phonon properties. The structure motif of the α phase is Ga_2 dimers, which form strong covalent bonds leading to bonding and antibonding states that suppress the density of states at the Fermi level. The β -Ga structure consists of arrays of Ga chains that favor strong coupling between the lattice vibrations and the electronic states near the Fermi level. The increased density of states and strong coupling to the phonons for the β -Ga chains compared to the α Ga_2 dimers enhance superconductivity in the β -Ga phase.

I. INTRODUCTION

The structural phase diagram of elemental gallium is complex. At ambient pressure, gallium crystallizes in the stable orthorhombic α phase. Several metastable phases, β , γ , δ , and ϵ , can also be synthesized under ambient conditions.¹⁻⁴ Under pressure, Ga exhibits three additional phases, Ga-II, Ga-III, and Ga-V.^{5,6} Most gallium phases (α , β , γ , δ , Ga-II) undergo superconducting transitions. The superconducting transition temperature, T_c , of the stable α -Ga phase is about 0.9 K.⁷ However, the metastable β , γ , and δ phases have much higher T_c 's. Metastable β -Ga is reported to have a T_c of 5.9 to 6.2 K,⁸⁻¹⁰ while the transition temperatures of γ and δ Ga are 6.9 to 7.6 K^{10,11} and 7.85 K,¹² respectively.

The significant increase in the superconducting transition temperature from 0.9 K in the stable α phase to 5-8 K in the β , γ , and δ phases poses an interesting theoretical question. In the context of the recent discoveries of high-temperature superconductivity in hydrides at megabar pressure,¹³ there is great interest in understanding situations where long-lived metastable phases formed at ambient or high pressure might exhibit a higher T_c than their stable counterparts. The gallium phases represent a unique opportunity to study this problem theoretically to understand the enhancement from the low- T_c stable phase to the higher- T_c metastable phases.

The phase stability of gallium was first studied by Gong *et al.* and Bernasconi *et al.* separately in the 1990s.^{14,15} Both studies found that the α structure is the most stable phase. Gong *et al.* pointed out that the structural motif of α -Ga consists of Ga_2 dimers with strong covalent bonding and significant charge localization inside the dimers. A recent study based on the Wannier functions analysis of the chemical bonding in α -Ga also supports covalent bonds within the Ga_2 dimers.¹⁶ Gong *et al.* characterize the metallic α -Ga phase with its strong Ga-Ga bonds as “a metallic molecular crystal”.¹⁴

Recently, Campanini *et al.* reported an *in situ* characterization of the α to β phase transition using a membrane-based nanocalorimeter⁹ and found that β -Ga is a strong coupling type-I superconductor with a T_c of around 6 K.⁹ Khasanov *et al.* measured the thermodynamic critical field and specific heat of the high-pressure Ga-II phase as a function of temperature and demonstrated that it follows the same universal relations as in conventional superconductors.¹⁷ The significant improvement in T_c as a result of the structure phase transition from the stable α structure to the metastable β structure motivates us to examine various aspects of the two phases in search of factors that are important for improving T_c . In principle it would be interesting to study the even higher- T_c γ and δ phases as well, but the unit cell of these phases contain 20 and 66 atoms per primitive cell, respectively. By contrast, the primitive cells of the α and β phases, contain 4 and 2 atoms, respectively.

This paper is structured as follows. Section II describes the details of the density-functional theory (DFT) calculations and the crystal structure of α and β gallium. Section III compares the electronic structure, charge density distribution, and electron-phonon coupling for the α and β phases of gallium. We show that the covalent Ga_2 dimers in α -Ga suppress the electronic density of states (DOS) at the Fermi level, E_f , and that the chains in β -Ga lead to electronic states near E_f that strongly couple to the phonons, thereby, increasing the superconducting transition temperature. Section IV, V summarize the results and discuss possible routes for improving the T_c of elemental gallium.

II. COMPUTATIONAL METHOD AND CRYSTAL STRUCTURE

We perform the DFT calculations using the Quantum Espresso code¹⁸⁻²⁰ with optimized norm-conserving

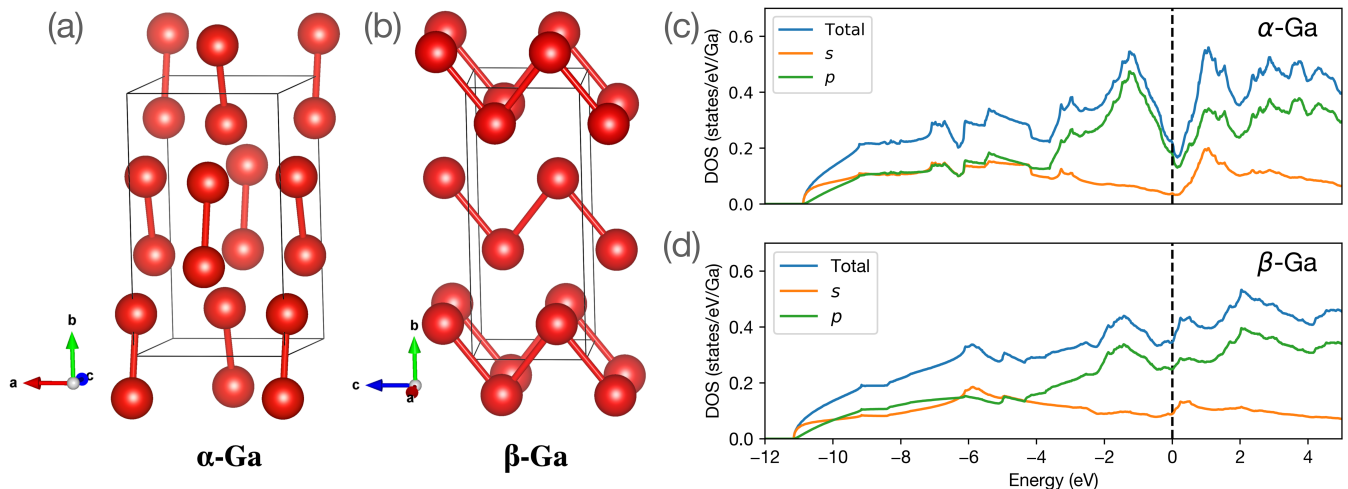


FIG. 1. The crystal structure (a,b) and electronic density of states (c,d) of α and β Ga. In the α phase (a), Ga atoms form dimers (or dumbbells), which lead to bonding and antibonding states that suppress the density of states at the Fermi level (c). In the β phase (b), the Ga atoms form arrays of one-dimensional chains along the \bar{c} lattice vector direction that result in an increased density of states at the Fermi level (d).

pseudopotential^{21,22} and the PBE generalized gradient exchange-correlation functional.²³ The plane-wave cutoff is set to 80 Ry and the charge density cutoff to 320 Ry. The k -point mesh for the self-consistent calculations is $25 \times 25 \times 25$ and the q -point mesh for the electron-phonon coupling calculations is $5 \times 5 \times 5$. After computing ϵ_k , ω_q , and $g(k, q)$ on a coarse mesh, we construct the electron and phonon Wannier functions using the EPW code^{24,25} to interpolate onto fine k and q meshes with $60 \times 60 \times 60$ and $30 \times 30 \times 30$ points, respectively.

Figure 1 (a) and (b) show the orthorhombic α and the monoclinic β gallium phases with space groups $Cmca(64)$ and $C2/c(15)$, respectively. The DFT relaxed lattice parameters for the α phase are $a = 4.55$, $b = 7.71$, and $c = 4.56$ and for the β are $a = 2.79$, $b = 8.09$, and $c = 3.34$, and $\beta = 92.2^\circ$, which are within 2% of the experimental values for the lengths of the lattice vectors and within 0.2° for the monoclinic angle.^{2,14}

III. RESULTS

Electronic structure. The electron configuration of the gallium atom is $[Ar]3d^{10}4s^24p^1$, with a filled $3d$ shell that does not participate in the chemical bonding. The $4s$ and $4p$ states hybridize and form bonds between the Ga atoms. Although the valence states of α and β -Ga consist of the same $4s$ and $4p$ orbitals, the bonding states and their orbital character near the Fermi level differ substantially in the two phases. Figure 1(c) shows that in α -Ga, states within 2 eV below the Fermi level are predominantly $4p$ states with negligible $4s$ character, while the $4s$ orbital contributes to one-third of the total DOS within 2 eV above the Fermi level. For β -Ga shown in Fig. 1 (d), the $4p$ orbitals dominate the DOS within 2 eV above and below the Fermi level, and the variation in

DOS near the Fermi level is small. The most important feature in the DOS of α -Ga is the V-shaped pseudogap at the Fermi level that substantially reduces the number of states near E_f . This pseudogap has been attributed to covalent bonding,^{14,15} the crystal structure of the α phase,²⁶ and the interplay between the electronic states and the Brillouin zone geometry.²⁷

Figure 2 shows how the band structures of α and β -Ga differ in several aspects that lead to the observed pseudogap in α -Ga and a larger DOS in the β phase. The electronic structure of the β -Ga consists of free-electron-like parabolic bands that span a few eV due to strong intra-chain and inter-chain hoppings. The band structure of the α -Ga, on the other hand, has a few bands that are dispersionless along certain k -paths in the Brillouin zone. The flat bands at 1.5 eV below the Fermi level along $X - S - R$ contributes to the DOS peak at -1.5 eV. The DOS peak at 1 eV originates from the flat bands along $\Gamma - X - S$.

Fig. 3 illustrates the Fermi surfaces of the α and β -Ga. The Fermi surface of α -Ga is continuous across the entire Brillouin zone along the $\bar{a}^* + \bar{b}^*$ and \bar{c}^* directions. Along the $\bar{a}^* - \bar{b}^*$ direction, the Fermi surfaces is confined to the region from $-0.2(\bar{a}^* - \bar{b}^*)$ to $+0.2(\bar{a}^* - \bar{b}^*)$, see Fig. S1 in the supplement for detail. The Fermi surfaces of β -Ga extend throughout the Brillouin zone and exhibit flat regions due to its one dimensional chain-like crystal structure, which in part explains the metastability of the β phase.

Charge density distributions. The pseudogap in the α -Ga DOS near the Fermi level strongly suggests the formation of filled bonding and empty antibonding states. Figures 4(a) and (b) show cuts through the charge density of α -Ga that include the Ga_2 dimer for the energy windows $[-1.5 \text{ eV}, -0.5 \text{ eV}]$ and $[0.5 \text{ eV}, +1.5 \text{ eV}]$, respec-

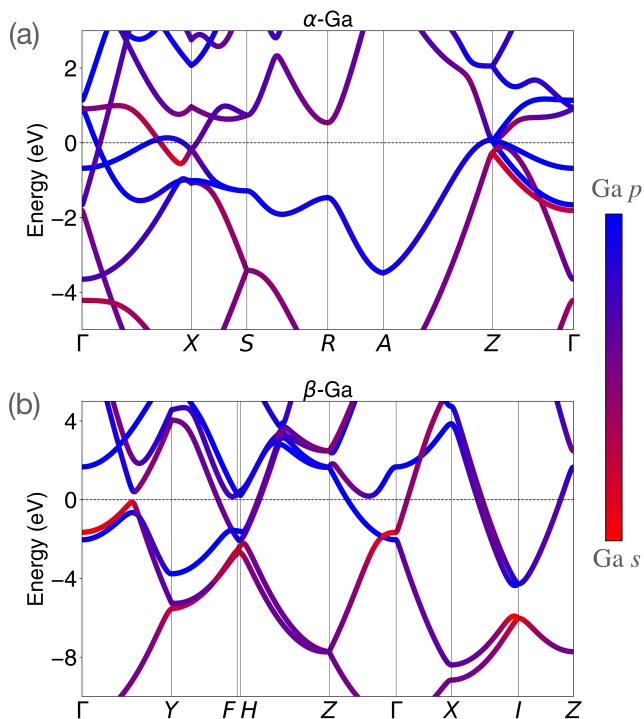


FIG. 2. The band structures of α and β -Ga projected on the $4s$ and $4p$ atomic orbitals show several nearly flat bands in the α -Ga and nearly free-electron parabolic bands for β -Ga.

tively. The maximum in the charge density between the dimers for the states below the Fermi level and the valley for the states above demonstrate bonding and antibonding states below and above the Fermi level, respectively. Therefore, the formation of strong covalent bonds for the α -Ge dimers results in localized states that are shifted away from the Fermi level and, hence, do not participate in the electron-phonon coupling process.

In contrast to α -Ga, Figures 4 (c) and (d) show that β -Ga displays a delocalized charge density along the Ga chains. Therefore, the breaking of the Ga dimers liberates the electronic states from the localized molecular bonds, leading to an increased number of states available near the Fermi level that can couple to the lattice vibrations and increase superconductivity.

Phonon dispersion and electron-phonon coupling. To identify the phonon modes that strongly couple to the electronic states, we plot the phonon dispersion of β -Ga in Fig. 5(a) along the high-symmetry path with the symbol sizes representing the electron-phonon coupling strength $\lambda_{\vec{q}}^{\nu}$, where ν denotes the phonon branch index and \vec{q} the wavevector. The two lowest acoustic phonon branches display large electron-phonon coupling $\lambda_{\vec{q}}^{\nu}$ with noticeable variation along the high-symmetry path. We calculate the mean and standard deviation of $\lambda_{\vec{q}}^{\nu}$ for each phonon branch to quantify the strength and anisotropy of the electron-phonon coupling. Table I shows that the average coupling strength of the lowest two phonon branches are 0.36 and 0.25, which accounts for half of the

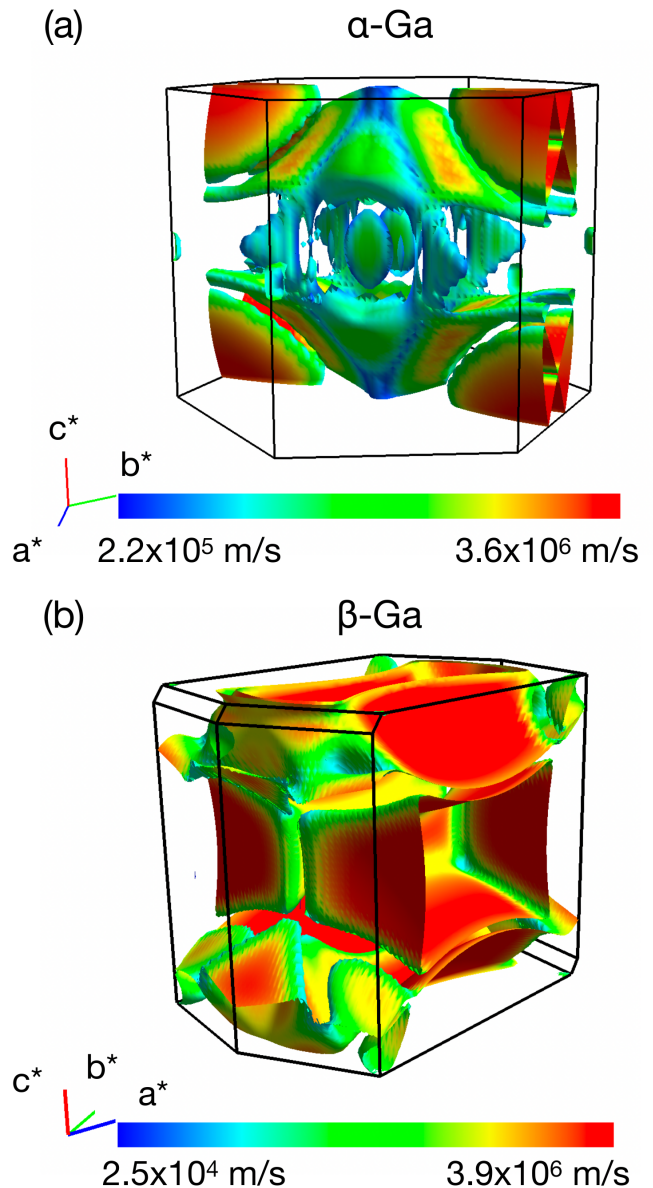


FIG. 3. The Fermi surfaces of the (a) α and (b) β -Ga. Color indicates the Fermi velocity.

total coupling strength of 1.16. The coupling constants of the third and fourth branches are 0.16 and 0.15, respectively, about 27% of the total coupling strength, and the highest two phonon branches contribute 19% of the total coupling.

Figure 5(b) compares the calculated electron-phonon coupling $\alpha^2F(\omega)$ obtained with the EPW code for the fine k and q -point meshes with the experimental $\alpha^2F(\omega)$ from tunneling experiments²⁸ for β -Ga. The excellent agreement validates the computational methodology. Table II summarizes the electron-phonon coupling strength λ and the frequency moments $\langle\omega_2\rangle$ and $\langle\omega_{\log}\rangle$ of β -Ga. Using the Allen-Dynes equation with $\mu^* = 0.13$, we esti-

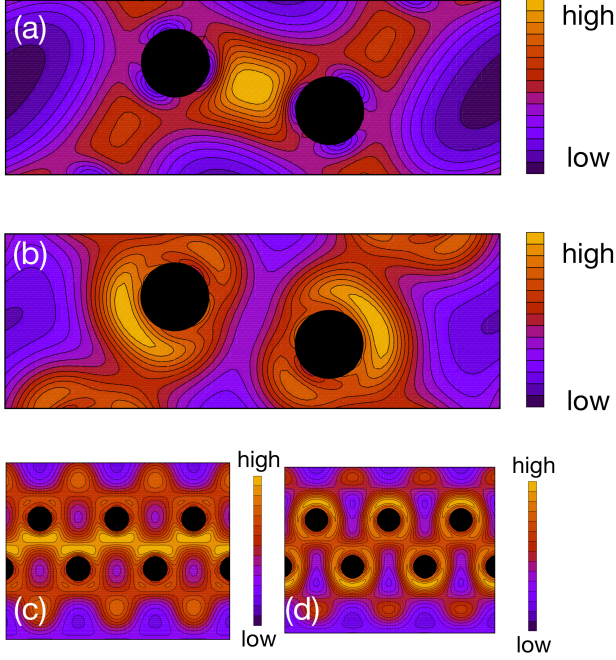


FIG. 4. Charge density of α and β -Ga projected on 1 eV energy windows surrounding the Fermi level. The charge densities for α -Ga demonstrate the presence of localized (a) bonding and (b) antibonding states between the Ga_2 dimers within 1 eV of the Fermi level. For the β phase, the charge densities (c) and (d) are delocalized along the Ga-chain, indicating one-dimensional extended states that couple strongly to the lattice.

TABLE I. The mean and standard deviation of λ_q^ν integrated over the entire Brillouin zone for each phonon branch ν and in total. The electron-phonon coupling of the lowest branch is as large as the sum of the highest three branches.

Phonon branch ν	1	2	3	4	5	6	Total
Mean $\langle \lambda_q^\nu \rangle_q$	0.36	0.25	0.16	0.15	0.12	0.10	1.13
Standard deviation	0.34	0.11	0.07	0.08	0.04	0.04	0.43

mate a superconducting transition temperature of 6.5 K. Solving the isotropic Eliashberg equations, we obtain essentially the same superconducting transition temperature of 6.6 K. These values closely match the reported experimental T_c of 5.9 to 6.2 K.^{8–10} To characterize the anisotropy of the superconductivity, we also solve the anisotropic Eliashberg equations at several temperatures below T_c . Figure 6 compares the isotropic and anisotropic gap function as a function of temperature, which demonstrates that β -Ga is an isotropic superconductor.

Figures 7 and 8 illustrate the phonon spectrum and the eigenmodes at Γ for α -Ga, respectively. The primitive cell of the α -Ga structure contains four atoms that all lie on the $\vec{b}-\vec{c}$ plane, which represents a mirror plane. As a result, there are two types of phonon modes at the Γ point, in-plane and out-of-plane vibrations, as shown in Fig. 8. The first and the sixth optical phonon modes

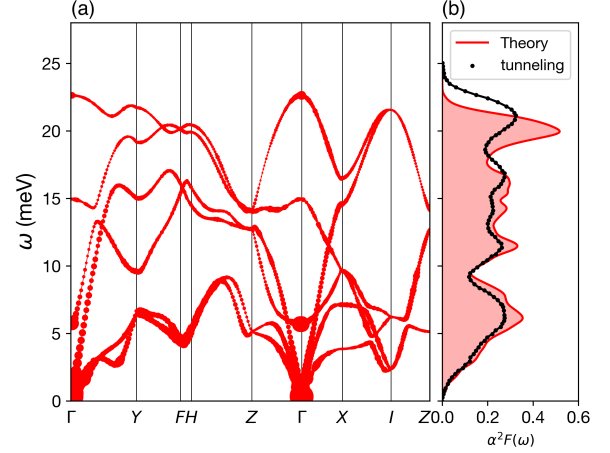


FIG. 5. (a) Phonon dispersion of β -Ga with the size of the data points proportional to λ_q^ν and (b) comparison of $\alpha^2 F(\omega)$ obtained from DFT calculations (red) with experimental tunneling data (black) from Ref. 28.

TABLE II. Calculated electron-phonon coupling parameters λ , $\langle \omega_2 \rangle$, $\langle \omega_{\log} \rangle$, and Allen-Dynes critical temperature T_c^{AD} for $\mu^* = 0.13$ of α and β -Ga. The tunneling data, $\lambda^{\text{tunneling}}$, is from Ref. 28.

	λ^{theory}	$\lambda^{\text{tunneling}}$	$\langle \omega_2 \rangle$ (meV)	$\langle \omega_{\log} \rangle$ (meV)	T_c^{AD} (K)
α -Ga	0.39	—	15.6	12.2	0.23
β -Ga	1.16	0.97	10.7	6.9	6.5

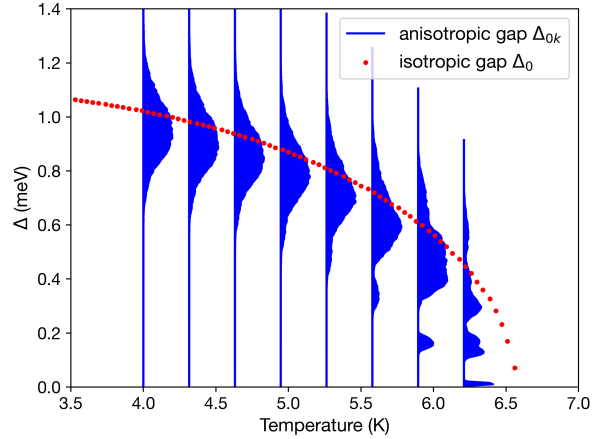


FIG. 6. Comparison of the isotropic gap function (red) and the anisotropic gap function (histogram of gap values over the Fermi surface, blue) as a function of temperature shows that β -Ga is well described as an isotropic superconductor.

comprise of out-of-plane Ga-Ga bond bending, while for the third optical phonon mode, the two Ga-Ga dimers vibrate rigidly into and out of the $\vec{b}-\vec{c}$ plane. The second and the seventh optical phonon modes are the in-plane counterparts of the third optical mode. The eighth and

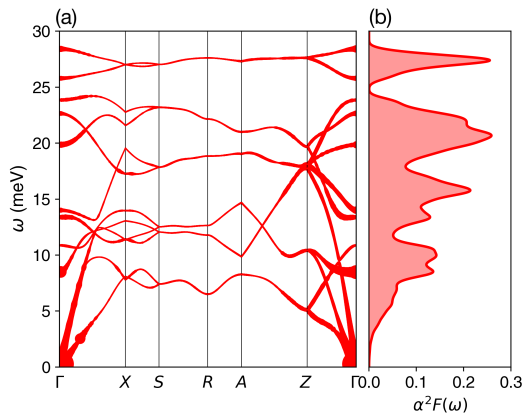


FIG. 7. (a) Phonon dispersion of α gallium along high symmetry path. (b) Eliashberg function of α gallium.

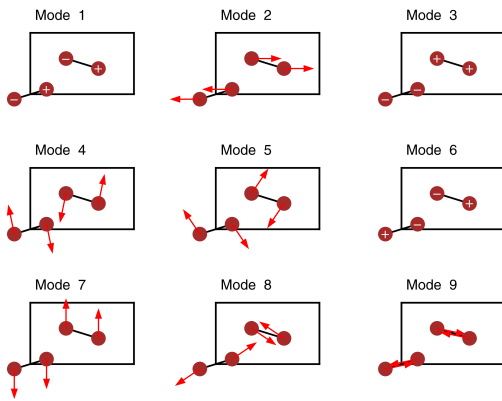


FIG. 8. The nine optical phonon modes at the Γ point for the α -Ga. The plus and minus signs indicate the motion perpendicular to the plane. The two highest frequency modes (mode 11 and 12) are in-phase and out-of-phase Ga-Ga bond stretching modes, respectively.

the ninth phonon modes are bond stretching modes with much higher frequencies than the in-plane bond bending modes (modes 4 and 5). In addition, the phonon dispersions of the highest two phonon branches are gapped from the rest of the phonon spectrum, see Fig. 7. The integration of $g(\omega) = \frac{2\alpha^2 F(\omega)}{\omega}$ over the frequency range from 25 to 30 meV turns out to be 0.03, about 13% of the total electron-phonon coupling strength.

IV. DISCUSSION

Several members in the boron group have played an important role in the quest for high-temperature superconductivity. Boron in MgB_2 , for example, has p orbitals that form delocalized metallic σ and π bonds. Although α -Ga has strong bonds, they are localized and either below or above the Fermi level. Electron or hole doping might shift the Fermi level towards the DOS peaks at +1 or -1.5 eV, respectively, which could improve the superconducting transition temperature of the stable α phase.

Applying external pressures could be another route for improving the superconducting transition temperatures of α and β -Ga. Elemental boron *per se* is not a superconductor under ambient conditions, although it can transform into a superconductor with a T_c of 4 K at 160 GPa. Further increasing the external pressure to 250 GPa can improve the T_c to 11 K.²⁹

Gallium is already a superconductor at ambient pressure. Its T_c ranges from 1 K in the stable α phase to 5-7 K in the metastable β , γ , δ phases. Under external pressure, several new phases are predicted to form.³⁰⁻³² The superconductivity of Ga-II, one of several phases of gallium that emerge under pressure, is measured to be 6.46 K at 3.5 GPa.¹⁷ But the superconductivity of gallium under megabar pressures has not been explored systematically. Given that boron, the lightest member of the boron group, undergoes several structure phase transitions before it arrives at its superconducting phase under 160 GPa, new Ga phases with higher T_c might also emerge under extreme pressure.

V. SUMMARY

We demonstrated that the disparate superconducting properties of gallium's α and β phases originate from their difference in bonding using DFT and presented first-principles calculations of the electronic structure, phonon dispersion, electron-phonon coupling, and superconducting properties. For the α phase, the Ga_2 dimers form bonding and antibonding states that result in a V -shaped suppression of the DOS at the Fermi level, which significantly reduces the number of states available for coupling to the phonons. The DOS of metastable β -Ga, on the other hand, is nearly free-electron gas-like due to strong intra- as well as inter-chain hoppings. The charge density confirms the strongly localized bonding and antibonding states below and above the Fermi level in α -Ga, while it shows delocalized states near the Fermi level in β -Ga that are more likely to respond to lattice vibrations. The T_c of β -Ga is estimated to be 6.5 K, which agrees with the experimental values of 5.9 to 6.2 K⁸⁻¹⁰ and is much higher than the T_c of α Ga. Also, the calculated electron-phonon coupling $\alpha^2 F(\omega)$ for β -Ga closely matches experiment,²⁸ validating the computational approach. Therefore, the formation of Ga_2 dimers in the α phase suppresses its superconductivity.

We hope that this understanding of the electronic and phononic structure of the higher- T_c metastable β Ga phase can pave the way to understanding and designing ambient pressure metastable phases of other superconductors with higher T_c s.

VI. ACKNOWLEDGEMENTS

The work was supported by the US Department of Energy Basic Energy Sciences under Contract No. DE-SC-0020385. This research used computational resources

provided by the University of Florida Research Computing and the Texas Advanced Computing Center under Contracts TG-DMR050028N. This work used the Ex-

treme Science and Engineering Discovery Environment (XSEDE), which is supported by National Science Foundation grant number ACI-1548562.

- ¹ B. D. Sharma and J. Donohue, *Zeitschrift für Kristallographie* **117**, 293 (1962).
- ² L. Bosio, A. Defrain, H. Curien, and A. Rimsky, *Acta Crystallographica Section B* **25**, 995 (1969).
- ³ L. Bosio, H. Curien, M. Dupont, and A. Rimsky, *Acta Crystallographica Section B* **28**, 1974 (1972).
- ⁴ L. Bosio, H. Curien, M. Dupont, and A. Rimsky, *Acta Crystallographica Section B* **29**, 367 (1973).
- ⁵ L. Bosio, *The Journal of Chemical Physics* **68**, 1221 (1978).
- ⁶ O. Degtyareva, M. I. McMahon, D. R. Allan, and R. J. Nelmes, *Phys. Rev. Lett.* **93**, 205502 (2004).
- ⁷ B. Chen, X. Duan, H. Wang, J. Du, Y. Zhou, C. Xu, Y. Zhang, L. Zhang, M. Wei, Z. Xia, C. Cao, J. Dai, M. Fang, and J. Yang, *npj Quantum Materials* **3**, 40 (2018).
- ⁸ H. Parr and J. Feder, *Phys. Rev. B* **7**, 166 (1973).
- ⁹ D. Campanini, Z. Diao, and A. Rydh, *Phys. Rev. B* **97**, 184517 (2018).
- ¹⁰ J. Feder, S. Kiser, F. Rothwarf, J. Burger, and C. Valette, *Solid State Communications* **4**, 611 (1966).
- ¹¹ L. Bosio, R. Cortes, A. Defrain, and I. Epelboin, *C. R. Acad. Sci. (Paris)* **264B** (1967).
- ¹² L. Bosio, R. Cortes, A. Defrain, and I. Epelboin, *C. R. Acad. Sci. (Paris)* **268B**, 1314 (1969).
- ¹³ J. A. Flores-Livas, L. Boeri, A. Sanna, G. Profeta, R. Arita, and M. Eremets, *Physics Reports* **856**, 1 (2020), a perspective on conventional high-temperature superconductors at high pressure: Methods and materials.
- ¹⁴ X. G. Gong, G. L. Chiarotti, M. Parrinello, and E. Tosatti, *Phys. Rev. B* **43**, 14277 (1991).
- ¹⁵ M. Bernasconi, G. L. Chiarotti, and E. Tosatti, *Phys. Rev. B* **52**, 9988 (1995).
- ¹⁶ R. C. Remsing, J. Sun, U. V. Waghmare, and M. L. Klein, *Molecular Physics* **116**, 3372 (2018).
- ¹⁷ R. Khasanov, H. Luetkens, A. Amato, and E. Morenzoni, *Phys. Rev. B* **101**, 054504 (2020).
- ¹⁸ P. Giannozzi, O. Andreussi, T. Brumme, O. Bunau, M. B. Nardelli, M. Calandra, R. Car, C. Cavazzoni, D. Ceresoli, M. Cococcioni, N. Colonna, I. Carnimeo, A. D. Corso, S. de Gironcoli, P. Delugas, R. A. DiStasio, A. Ferretti, A. Floris, G. Fratesi, G. Fugallo, R. Gebauer, U. Gerstmann, F. Giustino, T. Gorni, J. Jia, M. Kawamura, H.-Y. Ko, A. Kokalj, E. Küçükbenli, M. Lazzeri, M. Marsili, N. Marzari, F. Mauri, N. L. Nguyen, H.-V. Nguyen, A. O. de-la Roza, L. Paulatto, S. Poncé, D. Rocca, R. Sabatini, B. Santra, M. Schlipf, A. P. Seitsonen, A. Smogunov, I. Timrov, T. Thonhauser, P. Umari, N. Vast, X. Wu, and S. Baroni, *Journal of Physics: Condensed Matter* **29**, 465901 (2017).
- ¹⁹ P. Giannozzi, S. Baroni, N. Bonini, M. Calandra, R. Car, C. Cavazzoni, D. Ceresoli, G. L. Chiarotti, M. Cococcioni, I. Dabo, A. D. Corso, S. de Gironcoli, S. Fabris, G. Fratesi, R. Gebauer, U. Gerstmann, C. Gougoussis, A. Kokalj, M. Lazzeri, L. Martin-Samos, N. Marzari, F. Mauri, R. Mazzarello, S. Paolini, A. Pasquarello, L. Paulatto, C. Sbraccia, S. Scandolo, G. Sclauzero, A. P. Seitsonen, A. Smogunov, P. Umari, and R. M. Wentzcovitch, *Journal of Physics: Condensed Matter* **21**, 395502 (2009).
- ²⁰ P. Giannozzi, O. Baseggio, P. Bonfà, D. Brunato, R. Car, I. Carnimeo, C. Cavazzoni, S. de Gironcoli, P. Delugas, F. Ferrari Ruffino, A. Ferretti, N. Marzari, I. Timrov, A. Urru, and S. Baroni, *The Journal of Chemical Physics* **152**, 154105 (2020).
- ²¹ D. R. Hamann, *Phys. Rev. B* **88**, 085117 (2013).
- ²² M. Schlipf and F. Gygi, *Computer Physics Communications* **196**, 36 (2015).
- ²³ J. P. Perdew, K. Burke, and M. Ernzerhof, *Phys. Rev. Lett.* **77**, 3865 (1996).
- ²⁴ J. Noffsinger, F. Giustino, B. D. Malone, C.-H. Park, S. G. Louie, and M. L. Cohen, *Computer Physics Communications* **181**, 2140 (2010).
- ²⁵ S. Poncé, E. Margine, C. Verdi, and F. Giustino, *Computer Physics Communications* **209**, 116 (2016).
- ²⁶ E. Voloshina, K. Rosciszewski, and B. Paulus, *Phys. Rev. B* **79**, 045113 (2009).
- ²⁷ Z. Y. Zhu, Y. C. Cheng, and U. Schwingenschlögl, *Journal of Physics: Condensed Matter* **23**, 475502 (2011).
- ²⁸ J. P. Garno, *Review of Scientific Instruments* **49**, 1218 (1978).
- ²⁹ M. I. Eremets, V. V. Struzhkin, H.-k. Mao, and R. J. Hemley, *Science* **293**, 272 (2001).
- ³⁰ R. Li, L. Wang, L. Li, T. Yu, H. Zhao, K. W. Chapman, Y. Wang, M. L. Rivers, P. J. Chupas, H.-k. Mao, and H. Liu, *Scientific Reports* **7**, 5666 (2017).
- ³¹ T. Yu, J. Chen, L. Ehm, S. Huang, Q. Guo, S.-N. Luo, and J. Parise, *Journal of Applied Physics* **111**, 112629 (2012).
- ³² J. W. E. Drewitt, F. Turci, B. J. Heinen, S. G. Macleod, F. Qin, A. K. Kleppe, and O. T. Lord, *Phys. Rev. Lett.* **124**, 145501 (2020).

Supplementary material

Yundi Quan,^{1,2,3} P. J. Hirschfeld,¹ and R. G. Hennig^{2,3}

¹*Department of Physics, University of Florida, Gainesville, Florida 32611, USA*

²*Department of Materials Science and Engineering,
University of Florida, Gainesville, Florida 32611, USA*

³*Quantum Theory Project, University of Florida, Gainesville, Florida 32611, USA*

I. FERMI SURFACES

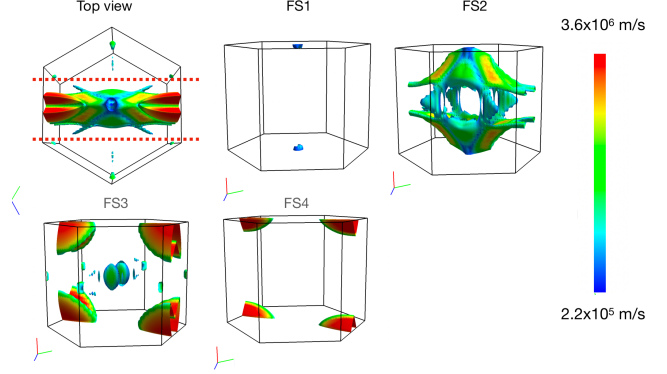


FIG. S1: The Fermi surfaces of the α gallium are shown in the figure above. FS1 to FS4 correspond to the four bands that cross the Fermi level.

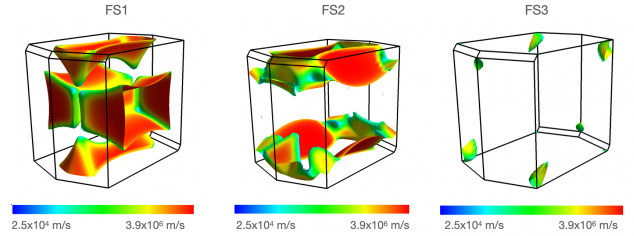


FIG. S2: The Fermi surfaces of the β gallium corresponding to the three bands that cross the Fermi level are shown in the figure above.

II. PHONON MODES

The Fermi surfaces of the α and the β gallium are presented in Fig. S1 and Fig. S2 respectively. The Fermi surfaces of the α gallium are mostly confined inside a region between $-0.2(\vec{a}^* - \vec{b}^*)$ to $0.2(\vec{a}^* - \vec{b}^*)$, see Fig. S1.

We have visualized the lowest two phonon modes of β -Ga at Y and F points, see F1.mp4, F2.mp4, Y1.mp4 and Y2.mp4, which help understand the collective Ga vibrations that can induce strong electronic response. The phonon modes are visualized using [Phononweb](#).